Journal of Ecology

British Ecological Society

Journal of Ecology 2008, **96**, 569–580 doi: 10.1111/j.1365-2745.2008.01368.x

DISPERSAL SPECIAL FEATURE

Effects of canopy heterogeneity, seed abscission and inertia on wind-driven dispersal kernels of tree seeds

Gil Bohrer[1]†, Gabriel G. Katul[1,2], Ran Nathan[3], Robert L. Walko[1] and Roni Avissar[1]*

[1]*Department of Civil and Environmental Engineering;* [2]*Nicholas School of the Environment and Earth Science, Duke University, NC 27708, USA; and* [3]*Movement Ecology Laboratory, Department of Evolution, Systematics and Ecology, The Hebrew University of Jerusalem, Givat Ram, Jerusalem 91904, Israel*

Summary

1. Understanding seed dispersal by wind and, in particular, long-distance dispersal (LDD) is needed for management of plant populations and communities, especially in response to changes in climate, land use and natural habitats. Numerical models designed to explore complex, nonlinear atmospheric processes are essential tools for understanding the fundamental mechanisms involved in seed dispersal. Yet, thus far, nearly all such models have not explicitly accounted for the spatial heterogeneity that is a typical feature of all ecosystems.

2. The recently developed Regional Atmospheric Modelling System (RAMS)-based Forest Large Eddy Simulation (RAFLES) is used here to explore how within-stand canopy heterogeneity impacts LDD. RAFLES resolves microscale canopy heterogeneity such as small gaps and variable tree heights, and it simulates their impacts on turbulence inside and above the canopy in the atmospheric boundary layer (ABL). For that purpose, an Eulerian–Lagrangian module of seed dispersal is added to RAFLES to simulate seed trajectories.

3. Particular attention is paid to the sensitivity of statistical attributes of the dispersal kernels (i.e. mean, mode, variance, tail) to key simplifications common to all seed dispersal models, such as horizontal homogeneity in the canopy and flow field, and the tight coupling between air parcel trajectories and seed trajectories (i.e. neglecting seed inertia). These attributes appear to be sensitive to various factors operating at scales ranging from the seed scale to the ABL scale.

4. Simulations with RAFLES show that LDD is characterized by a dispersal kernel with a 'tail', asymptotically approaching a power law decay of –3/2 (mainly occurring for lighter seeds at high wind speeds). This is consistent with asymptotic predictions from analytical models. The wind speed threshold at which seed abscission occurs, set-up to be twice the standard deviation of the vertical wind speed, is shown to affect short-distance dispersal, but has no significant impact on LDD. Ignoring the effects of seed inertia on the seed trajectory calculations has a minor effect on short-distance dispersal and no effect on the probability of seed uplift. Thus, it has no significant impact on LDD.

5. *Synthesis*. Tree-scale canopy heterogeneity affects the turbulence characteristics inside and above the canopy and, consequently, this affects dispersal kernel statistics. A key finding from this study is that ejection is enhanced above the shorter trees of the canopy. Seeds dispersed above shorter trees have a higher probability of experiencing LDD while their short-distance dispersal remains practically the same. At inter-annual time scales, such interactions could affect species composition.

Key-words: canopy heterogeneity, Eulerian–Lagrangian simulation, heavy particle dispersal, land surface, large-eddy simulations, long-distance dispersal, seed dispersal by wind, spatial heterogeneity, spatial scale

†Present address: Center for the Environment, Harvard University, MA 02138, USA.
*Correspondence author. E-mail: avissar@duke.edu

Introduction

Interest in seed dispersal has risen rapidly over the last decade, motivated by the importance of this factor on the structure and dynamics of populations and communities (Nathan & Muller-Landau 2000; Levin *et al.* 2003; Levine & Murrell 2003). This is also motivated by the need to estimate, and possibly mitigate, anthropogenic effects such as biological invasions, conservation and transgene escape on plant populations (Trakhtenbrot *et al.* 2005; Williams *et al.* 2006; Wilson *et al.* 2007). In particular, rare long-distance dispersal (LDD) events are of disproportionate importance for population expansion following habitat or climate changes, and in meta-population dynamics (Clark *et al.* 1999, 2001; Nathan 2006). LDD events are anticipated to facilitate colonization of recently disturbed or new habitats, enable coexistence of competing species, affect population survival and genetic variability, and determine the consequences of management and conservation efforts (Kot *et al.* 1996; Higgins & Cain 2002; Volis *et al.* 2005).

Field studies have yielded important insights into complex dispersal processes (Levey *et al.* 2002; Forget *et al.* 2004). However, due to the inherent difficulty in observing and quantifying rare events, analytical, phenomenological and/or mechanistic models are the major tools currently available to study and predict LDD (Nathan *et al.* 2002, 2003; Kuparinen 2006; Nathan 2006). Early models used to study LDD include several simplifications on the canonical structure of the flow field and seed trajectories. Notably, these models use Eulerian higher-order closure techniques to represent the turbulence statistics needed for seed trajectory calculations (e.g. Katul & Albertson 1998; Katul & Chang 1999). Furthermore, they assume a tight coupling between the air parcel trajectories and seed trajectories. Earlier models often use three-dimensional (3D) Lagrangian trajectories forced by profiles of the first and second moments of the flow statistics (e.g. Poggi *et al.* 2006). Such trajectories are intended to reproduce observed dispersal kernels at relatively long (i.e. seasonal and annual) time scales. However, at these time scales, variation in meteorological conditions and leaf area density are substantial and, therefore, need to be considered.

Land-surface heterogeneity is likely to affect seed dispersal by wind, and LDD in particular (e.g. Nathan & Katul 2005; Nuttle & Haefner 2005; Schurr *et al.* 2008). Yet, except for a few preliminary attempts, mechanistic modelling of wind-dispersed seeds in 3D heterogeneous landscapes remains a major unresolved challenge, mostly because of the complexity of the nonlinear processes involved. Nonetheless, such a modelling capability is highly desirable to broaden our understanding of the fundamental mechanisms involved in dispersal processes in naturally heterogeneous and anthropogenically fragmented landscapes at the various scales. For simplification, and partly because detailed measurements of the 3D variability in leaf area density were not available, previous models have traditionally assumed planar-homogeneous flow. However, with recent advancements in remote sensing such as airborne canopy light detection and ranging (LIDAR) technologies, it is now feasible to obtain this information (Weishampel *et al.* 2000; Lefsky *et al.* 2002). Recently, Bohrer *et al.* (2007) proposed a novel technique to incorporate such massive and detailed data into numerical models.

Thus, a model that accounts for the landscape heterogeneity that is found in the real world is amenable to study a variety of important applications. For example, it has been hypothesized that within-stand canopy heterogeneity, such as variation in canopy height and crown densities, could promote differential arrival of wind-dispersed seeds to canopy gaps (e.g. Augspurger & Franson 1988). This remains to be demonstrated. The importance of accurately estimating dispersal kernels in heterogeneous landscapes has also been emphasized for assessing dispersal limitation as a factor structuring plant communities (Dalling *et al.* 2002).

In this study, the Regional Atmospheric Modelling System (RAMS)-based Forest Large-Eddy Simulation (RAFLES) (Bohrer 2007, hereafter referred to as 'B07') is used to explore how within-stand canopy heterogeneity impacts dispersal kernels and LDD. Large-eddy simulation (LES) is a numerical modelling technique that solves in space and time the conservation of mass, momentum and energy of a fluid, formulated by the Navier-Stokes equations (e.g. Avissar & Schmidt 1998). It resolves the 3D dynamic structures of the fluid or eddies, which are the building blocks of turbulent flow. In the atmospheric boundary layer (ABL), these eddies exist at a wide range of scales, from the height of that layer (up to a few kilometres), to the sub-millimetre viscous dissipation length scale. The kinetic energy associated with eddies smaller than the model resolution is represented through sub-grid scale (SGS) parameterization. LES is a reasonable compromise for the simulation of LDD events because heavy particles can be held aloft by short-lived bursts of strong vertical wind of small spatial scale, yet the domain relevant for these events is much larger than can be simulated with direct numerical simulations.

RAFLES is applicable to 3D, heterogeneous canopies and includes the effects of stem obstruction, leaf drag and canopy fluxes on the flow (see formulation in Supplementary Appendix S1). This state-of-the-art model is further enhanced here to include Eulerian–Lagrangian (E–L) transport of heavy particles.

Eulerian–Lagrangian transport models (e.g. Walko *et al.* 2001; Weil *et al.* 2004) use the combination of resolved Eulerian velocity from an atmospheric model, such as RAMS, and a parameterization of the SGS velocity, which includes a random component to account for the effects of SGS eddies. The effects of particle mass are accounted for through three mechanisms: (i) the addition of gravitational acceleration to the vertical particle movement; (ii) partial decoupling between the particle SGS velocity and the air SGS velocity due to the particle fall velocity and the particle inertia, as both limit the particle's ability to instantaneously follow velocity fluctuation; and (iii) the implementation of a drag force that moves the particle as a function of its velocity difference with the air. The third mechanism is typically ignored in E–L models, and by also ignoring inertia, these models assume that the

particle velocity is only a result of the air velocity and its fall velocity.

The main purpose of this paper is to explore the physical mechanisms that affect seed dispersal in general, and LDD in particular, in heterogeneous environments and across multiple spatial scales. Here, the performance of the E–L dispersal module of RAFLES is evaluated against mass seed release field experiments. Then, a numerical case study is used to explore how the canopy-top structure and the horizontal distribution of leaf area impact the dispersal kernels.

As explained in B07, the part of the canopy that has smaller trees is more prone to updraft anchoring. Based on these findings, we hypothesize that canopy heterogeneity, through its impact on turbulence, affects seed dispersal kernels. We also hypothesize that the probability of seed ejection above the canopy is increased near the shorter trees and, therefore, LDD is more likely from these trees.

Furthermore, we hypothesize that the minimal wind speed needed for abscission (hereafter referred to as 'AWS') affects dispersal. Particularly with light seeds, which are strongly coupled to the flow, a strong AWS is expected to promote seed uplifting in the same large eddies that lead to the seed abscission, and thereby increase LDD (Greene & Johnson 1992; Schippers & Jongejans 2005). Finally, seed inertia and temporal variation in drag force is commonly neglected in nearly all models. Here, we evaluate the importance of these neglected elements on seed dispersal.

Methods

EULERIAN–LAGRANGIAN SIMULATION OF SEED DISPERSAL

Formulation

The Einstein notation is used throughout the manuscript for vector equations (Supplementary Appendix S1). For this study, seeds are considered 'heavy particles' meaning that they have inertia, and they are moved as a result of the sum of forces created by gravity and drag between the particle surface and the fluid. A non-physical class of particles (i.e. virtual tracers) is added to the model to explore the relevance of ignoring inertia (e.g. Andersen 1991; Katul *et al*. 2005; Nathan & Katul 2005). The particle location, x_{pi}, is updated in time using the following set of equations:

$$\begin{cases} x_{\mathrm{pi}}^{(t+\Delta t)} = x_{\mathrm{pi}}^{(t)} + (u_{\mathrm{Li}}^{(t)} + \delta_{i3} v_t)\Delta t & \text{For virtual tracers – no inertia} \\ x_{\mathrm{pi}}^{(t+\Delta t)} = x_{\mathrm{pi}}^{(t)} + u_{\mathrm{pi}}^{(t+\Delta t)}\Delta t & \text{All other particle types} \\ u_{\mathrm{pi}}^{(t+\Delta t)} = u_{\mathrm{pi}}^{(t)} + a_{\mathrm{pi}}^{(t)}\Delta t & \\ a_{\mathrm{pi}}^{(t)} = [f_{\mathrm{D}}(u_{\mathrm{Li}}^{(t)} - u_{\mathrm{pi}}^{(t)}) - \delta_{i3} g][1 + f_{\mathrm{D}}\Delta t]^{-1} & \end{cases} \quad \text{eqn 1}$$

where u_{pi} is the particle velocity, a_{pi} is the particle acceleration, u_{Li} is the air velocity at the particle location, v_t is the particle terminal fall velocity (defined as the velocity of a free-falling object when the gravitational force is at equilibrium with the drag), and f_{D} is defined here as the particle drag frequency (see eqn 6 below). Superscript 't' represents present time, and Δt is the integration time step. The equation for acceleration is solved implicitly in time to avoid the numerical instability that can lead to 'rogue particle trajectories' (Yee & Wilson 2007), assuming the drag frequency and air velocity are constant over a single time step (0.02 s in this study). This balance formulation only accounts for the main forces – drag and gravity – on smooth objects. It neglects the possible aerodynamic effects of 'Bernouli sailing' (suggested by Horn *et al*. 2001), uplift on wing surfaces (Greene & Johnson 1989) and rotation (Azuma & Okuno 1987). Greene & Johnson (1990) determined that the rotational movement of seeds did not result in a nonlinear effect and can be parameterized by the terminal fall velocity. Though some of the other aerodynamic effects may be important, the grid scale needed to resolve these three effects is less than a millimetre and is therefore currently not feasible as part of a canopy-scale model. Some of the combined mean effects of these mechanisms are accounted for through the parameterization of the effective terminal velocity described in the next section.

The wind velocity at the particle location, u_{Li}, is the sum of the resolved, $\overline{u_{\mathrm{Li}}}$, and SGS, u'_{Li}, components. The resolved velocity is interpolated from the LES wind fields, and the SGS velocity is parameterized using a stochastic differential equation based on Thomson (1987), Weil *et al*. (2004) and Kim *et al*. (2005):

$$du'_{\mathrm{Li}} = -\frac{f_s u'_{\mathrm{Li}}}{T_{\mathrm{L}}^p}dt + \frac{1}{2}\left(\frac{1}{e}\frac{d\bar{e}}{dt}u'_{\mathrm{Li}} + \frac{2\partial\bar{e}}{3\partial x_i}\right)dt + \sqrt{\frac{4 f_s \bar{e}}{3T_{\mathrm{L}}^p}}d\xi_i \quad \text{eqn 2}$$

where $\bar{e}$ is the SGS turbulence kinetic energy (TKE), and $f_s = \tilde{e}/\tilde{E}$ expresses the importance of SGS TKE relative to the total (i.e. resolved + SGS) TKE, $\tilde{E}$. Note, a tilde marks a horizontal cross section averaging and time averaging over a period during which turbulence statistics are considered stationary (typically 30 min). $d\xi_i = N(0, \Delta t)$ is a random Gaussian increment. T_{L}^p is a Lagrangian time scale for the particle obtained by modifying the Lagrangian time scale for the air (Csanady 1963; Reynolds & Lo Iacono 2004; Weil *et al*. 2004) to include the effects of the particle's inertia

$$T_{\mathrm{L}}^P = \frac{4\bar{e}}{3C_0\varepsilon}\left(1 + \frac{3(\beta v_t)^2}{2\bar{e}}\right)^{-\frac{1}{2}} + \tau_p \quad \text{eqn 3}$$

where ε is turbulence dissipation (Supplementary Appendix S1, eqn A.12), τ_p is the particle relaxation time (defined as a property of the seed in eqn 5), β expresses the ratio between the Lagrangian and Eulerian time scales in the LES model and C_0 is the Kolmogorov constant for the Lagrangian structure function. Here, $\beta = 1.5$ (Sawford & Guest 1991), and $C_0 = 4$ (Thomson 1987) were used, although the exact value of both parameters remains a subject of active research (see Sawford & Guest 1991; Lien & D'Asaro 2002).

The probability of a seed to be intercepted by a canopy element, $I_p = 1 - \exp(-L_d\,|\,\Delta X_p\,|)$ is determined by the leaf area density in that element, L_d, and by the incremental path length of the seed through the canopy at each time step, $|\,\Delta X_p\,|$ (Raupach *et al*. 2001). When a seed is intercepted u'_{L} and u_p are zeroed. This represents a seed colliding with a leaf and continuing to fall. The effects of the aerodynamic shape of the seed on its probability of collision, and collisions with trunks are neglected. These might have a significant effect (Pounden *et al*. 2008) but, to date, no empirical data exist to allow incorporating these effects in the system we simulated here.

REPRESENTATION OF THE AERODYNAMIC PROPERTIES OF SEEDS

Wind-dispersed seeds have complex aerodynamic shapes. Common formulations assume small, smooth and spherical shapes and,

therefore, are not applicable for most seeds. In our formulation, we compare seeds to each other based on their mass, m_p, effective diameter, d_p and terminal fall velocity, v_t. These characteristics have frequently been reported for many species. Given that these characteristics are proportional to the drag acting on a seed, they can be used to determine the effective drag frequency and Lagrangian relaxation time, τ_p, which are needed to solve eqns 1–3. An analytical solution for v_t can be obtained from the equation of motion by assuming that the seed starts falling from rest in motionless air, and moving only in the vertical direction:

$$v_t = w_p \Big|_{\left(\frac{dw_p}{dt}=0\right)} = \left(\frac{m_p g}{\rho_{a0s} C_d A_p}\right)^{\frac{1}{2}} \quad \text{eqn 4}$$

where w_p is the vertical component of the particle velocity, C_d is the particle drag coefficient, A_p is the surface area of the particle, and $\rho_{a0s} = 1.23\ \text{kg m}^{-3}$ is the reference air density at the model ground level. The ground level air density is used here because in most cases, empirically observed values of v_t, which are substituted into eqn 4 to obtain the seeds drag coefficient, are measured near at the ground surface (and not at high altitudes).

For a large seed, τ_p is defined as the time it takes the seed to reach v_t from rest. It can be derived analytically from eqn 4:

$$\tau_p = \frac{v_t}{g}\left(\frac{\rho_{a0s}}{\rho_{a_0}}\right)^{\frac{1}{2}} \tanh^{-1}(\phi) \quad \text{eqn 5}$$

where ρ_{a_0} is the reference air density at the seed location. It is needed to account for changes in the terminal fall velocity due to the decreased air density at higher elevations. Because the fall velocity converges asymptotically to the terminal velocity, (i.e. $\lim^{w_p \to v_t}(t) = \infty$), a convergence parameter is defined as $\phi = w_p/v_t = 0.99$.

As many types of seeds can have Reynolds numbers much larger than unity when they are close to their terminal velocity (i.e. $Re > 10$), it is reasonable to formulate their drag coefficients in a similar manner to that of large objects. The instantaneous C_d is a nonlinear function of the slippage Reynolds number and the seed aerodynamic shape. This function is rarely known and depends on seed morphology. Aerodynamics studies in wind tunnels at a broad range of Re are needed to determine the drag function for each seed species. On average, $Re > 10$, and we therefore treat C_d as a constant. The particle drag frequency is accordingly, and based on eqn 4:

$$f_D = \frac{\rho_{a_0} C_d A_p}{m_p} |\mathbf{V}_L - \mathbf{V}_p| = \frac{\rho_{a_0}}{\rho_{a_0 s}} \frac{g}{v_t^2} |\mathbf{V}_L - \mathbf{V}_p| \quad \text{eqn 6}$$

where $|\mathbf{V}_L - \mathbf{V}_p|$ is the magnitude (scalar) of the difference between the air velocity and the particle velocity (often referred to as slippage velocity).

FIELD EXPERIMENT

Katul *et al.* (2005), hereafter referred to as 'K05', measured seed dispersal kernels in an 80–100-year-old second-growth oak hickory hardwood forest stand at the Black Division of the Duke Forest, near Durham, NC, USA. They manually released a large number of seeds of eight common wind-dispersed tree species. Additional details of the field experiment are provided in K05. Results from one of these manual release experiments were used for evaluation of the E–L component of RAFLES. The model's results were not significantly different than the kernels obtained in the field experiment (Supplementary Appendix S2).

NUMERICAL EXPERIMENT

Rationale

To simulate the ABL during a specific period, RAFLES must be forced with realistic, mean atmospheric conditions, which could be obtained from meteorological observations. When not available, a regional model (e.g. RAMS) can be used to provide these conditions. In its current version, RAFLES also requires the spatial distribution of surface fluxes (B07). In a new version under development, a multilayer energy balance equation is being introduced into RAFLES, which coupled to the atmospheric dynamics, will be able to calculate these fluxes.

Quite unfortunately, the spatial variability of these surface fluxes and atmospheric conditions aloft were not available for the days K05 performed their experiments. Thus, we had to choose between two less-than-optimal alternatives for our sensitivity analysis: (i) Approximate the surface fluxes in simulating the observations of K05; or (ii) use the simulations of B07, which were carefully crafted and evaluated, and proved to be reliable. These simulations were conducted for the same canopy used by K05, and it appears that the meteorological conditions adopted in their spring case were similar to those experienced by K05 on 13 May 2001. Therefore, we opted to use these simulations together with the observations collected by K05 on 13 May 2001. It is important to note that canopy structure has a major impact on turbulence across the entire flow domain and this structure did not change significantly between the time simulated by B07 and the field experiment of K05.

Large-eddy simulations

As explained above, the same atmospheric conditions and canopy structures used in B07 are used for our LES. The background atmospheric conditions, the atmospheric forcing, prescribed surface fluxes, and the vertical profiles of the simulated horizontal mean atmospheric variables are summarized in Supplementary Appendix S1 (Table A1.1, Fig. A1.1).

In the 'control' case, a heterogeneous canopy with the observed properties and structure of the hardwood stand used in K05 (McCarthy *et al.* 2007) was produced with the virtual canopy generator (V-CaGe) developed by Bohrer *et al.* (2007). V-CaGe mimics natural forests by generating 3D canopies in which the canopy top height and ground-accumulated leaf area index are correlated, as expected from the observed allometric relationship at the simulated forest stand. In the 'homogeneous' case, the same domain-averaged canopy properties were used but spatial variability was eliminated, resulting in a horizontally homogeneous canopy.

The model horizontal domain was $1280 \times 1280\ \text{m}^2$ with a mesh spacing of $5 \times 5\ \text{m}^2$. In the vertical, the domain extended up to 1460 m above ground level (AGL) with vertical mesh spacing of 3 m from the ground surface up to twice the mean canopy height. Above that height, the grid was stretched by a factor of 1.1 from grid level to grid level up to a maximal spacing of 30 m. The model time step was 0.02 s.

Virtual seed dispersal

Seeds were virtually released only after the initialization period was completed. A total of 6 528 000 seeds were released during the 25 min following the initialization period (Supplementary Appendix S1) in both the control and the homogeneous simulations. The virtual seeds were released at 40 locations as schematically illustrated in

Table 1. Mean terminal fall velocities (v_t), mean seed mass (m_p), and estimated mean length (d_p) of the simulated seed species from Katul *et al.* (2005)

Species	Common name	v_t (m s^{-1})	m_p (kg)	d_p (m)
Carpinus caroliniana	American hornbeam	1.89	5.46E-05	0.026
Fraxinus pennsylvanica	Green ash	1.43	5.13E-05	0.04
Acer saccharinum	Silver maple	1.10	16.50E-05	0.05
Acer rubrum	Red maple	0.67	1.81E-05	0.02

Supplementary Appendix S1 (Fig. A1.2). In the naturally heterogeneous 'control' case, the canopy height, h_c, varied over the domain between 16.1 and 39.4 m AGL. In the homogeneous case, h_c = 24.6 m everywhere, which corresponds to the mean height in the control case. The canopy height was produced by V-CaGe but lost some of its resolution when implemented into the grid of RAFLES. Trees characterized by different heights and locations were selected for the virtual seed release. At these locations, the canopy was either the highest (between 38.86 and 39.4 m), moderately high (30 ± 0.01 m), around the mean height (25 ± 0.01 m), or the lowest (between 16.1 and 17.0 m). For convenience, these locations are annotated as h_c = 39, 30, 25 or 17 m AGL, respectively. For each canopy height, 10 replicates at random locations with that height canopy were selected. At each location, seeds were released from four heights, z_r = 39, 30, 24 and 18 m AGL. These release heights are located at the centres of model grid cells. A small SGS component within the grid cell was added to the exact horizontal location of the release point, i.e. $x_{p0i} = x_{p0i} + U(\pm \Delta x_i/4)$ where i = 1, 2 (horizontal components only), a subscript '0' marks the release location, Δx is the horizontal grid spacing and $\boldsymbol{U}$ is a random uniform function. The exact same locations were used in the homogeneous canopy case.

In the real world (where canopies are heterogeneous), seed release above the height of the canopy top is possible. For example, a tall deciduous tree in a mixed forest releases seeds during the season that it is leafless, above the evergreen trees and understorey. Although this is not the case for the species tested in K05, the model results are not specific to these species (i.e. their precise drag and seed morphology is not employed) and can represent any other seed species with similar fall velocities and sizes.

Four virtual seed 'species' were used, with v_t of 0.67, 1.1, 1.43 and 1.89 m s^{-1}, based on those reported in K05. These terminal fall velocities were selected to obtain a broad range of v_t values, and correspond to the mean v_t reported for species used in the K05 field experiment. The characteristics of these seeds are summarized in Table 1. Other ecological and biological characteristics of these species, such as vertical and horizontal distribution of seed sources, release heights, conditions necessary for abscission, and seed maturation timing, were not treated explicitly. However, it should be emphasized that in K05, the seeds were released manually from the meteorological tower and did not reflect the species-specific release heights, abscission and maturation timing.

The total number of seeds virtually released in a simulation is a compromise between computational capability constraints and the need to sample as extensively as possible in space and time to account for the highly variable nature of turbulence and of the tail of the dispersal kernel. To bypass this constraint, a single value of terminal velocity was adopted for each representative virtual species, realizing that the lack of variability in this parameter was an unavoidable drawback of our study. Note, however, that K05 find a within-species coefficient of variation of v_t of about 20%, much smaller than the interspecies variation that is used here to compare kernels. Nathan & Katul (2005) reported that within-species variation of v_t is less important than interspecies variation and other variables such as release height and canopy density.

Each virtual seed species included four seed types, which were differentiated by their drag coefficient and abscission conditions: (i) 'Natural' seed, that is the control type, with the mean terminal fall velocity, mass and size as reported in K05 and with no minimal wind speed necessary for their abscission (i.e. AWS = 0 m s^{-1}); (ii) 'Tracer' seed, which are equivalent to the natural seed but have no inertia (see eqn 1); (iii) Low AWS seed, which are similar to the natural seed except AWS = 0.5 m s^{-1} (as in Williams *et al.* 2006); and (iv) High AWS seed, which are similar to the natural seed except AWS = 1.0 m s^{-1} (as observed in maple trees by Greene & Johnson 1992). Fifty seeds of each virtual species and type were virtually released at each location and each release height, every 30 s, during the 25-min numerical experiments. This release frequency was selected to match that of K05.

Data analysis

The release and settling locations of all seeds were recorded. A histogram of the dispersal distances was built for each seed type, release location and release height. These histograms, intended to approximate the dispersal kernel, consisted of 200 bins. In cases when the farthest dispersed seed travelled < 100 m, the width of all bins was 0.5 m. Otherwise, the first 100 bins were 0.5-m wide, and the other 100 bins equally divided the space between 50 m and the distance of the farthest seed. The histograms were normalized by the bin width and total sample size to produce the dispersal kernel.

Throughout this paper, the term dispersal kernel is used to represent the one-dimensional (binned) probability of a seed to travel the distance from the seed release point to its deposition site (that falls within the bin limits), averaged over all seeds from all sources with the same characteristics in a specific LES. We do not consider pre- or post-dispersal processes that affect, for example, seed viability and germination. The statistical properties of the dispersal kernel (i.e. mean, mode, variance, tail) are used to compare the numerical experiments. The median and mode of the kernel were used to quantify short-distance dispersal because they are independent of the tail of the dispersal kernel. We define LDD by combining its proportional and absolute definitions (Nathan 2005), using the average distance travelled by the 0.01-percentile of the furthest reaching seeds, and the probability of dispersing further than 100 m, respectively.

Results

MEAN DISPERSAL KERNELS

As can be expected, the simulated dispersal kernels of 'natural' seeds (Fig. 1) show that slower terminal velocity (v_t) and

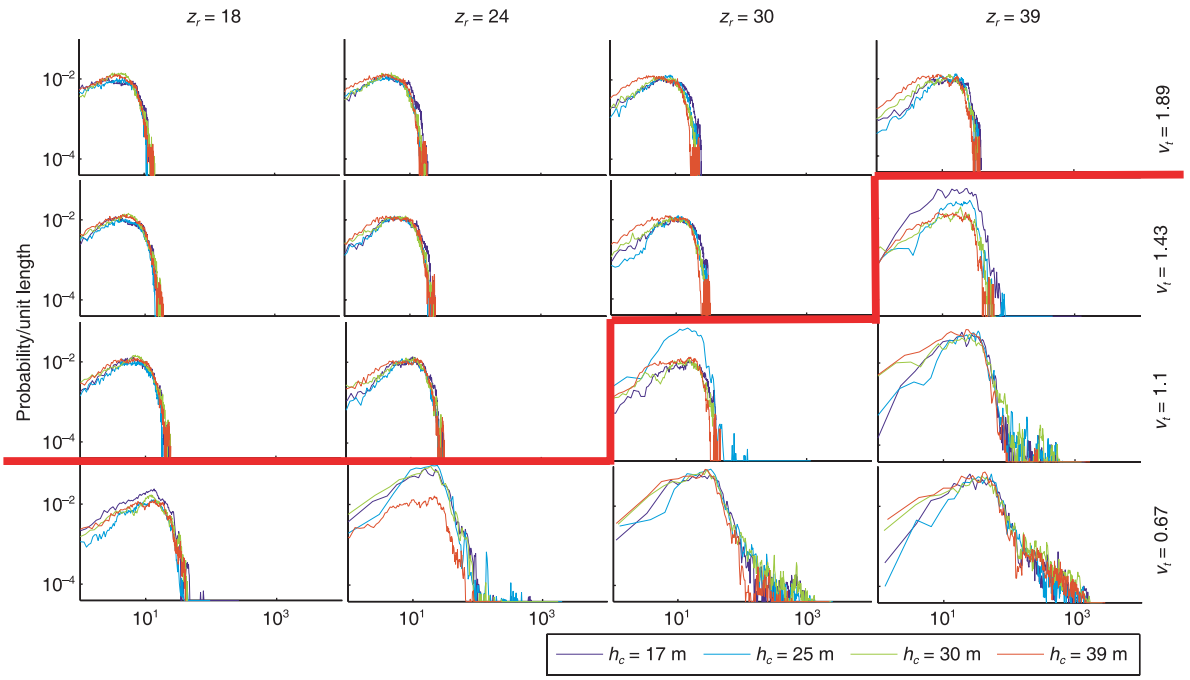

Fig. 1. Simulated dispersal kernels for the heterogeneous canopy, with different terminal velocities (v_t, m s^{-1}) and release heights (z_r, m AGL). Note the logarithmic scale in both axes. The solid red line separating the frames indicates the 'LDD divide'.

Table 2. Decay rate of the dispersal kernel tail. Cases that displayed some degree of LDD (see Fig. 1) are in bold

		h_c (m)			
z_r (m)	v_t (m s^{-1})	17	25	30	39
18	1.89	–5.3	–6.3	–6.0	–6.6
	1.43	–5.1	–4.7	–4.9	–5.9
	1.1	–4.9	–4.4	–4.8	–5.2
	0.67	**–4.3**	–5.4	–4.0	–4.0
24	1.89	–5.4	–5.7	–5.4	–6.0
	1.43	–4.9	–4.6	–5.0	–5.3
	1.1	–5.0	–4.5	–4.6	–5.2
	0.67	**–2.1**	**–2.0**	**–2.5**	–4.6
30	1.89	–3.5	–4.7	–4.7	–5.5
	1.43	–3.6	–4.6	–4.7	–5.4
	1.1	–3.6	**–2.7**	–3.9	–5.4
	0.67	**–1.7**	**–1.9**	**–1.7**	**–2.0**
39	1.89	–3.8	–5.7	–4.6	–4.5
	1.43	**–2.9**	**–5.6**	–5.4	–4.8
	1.1	**–2.0**	**–2.1**	**–2.3**	**–2.2**
	0.67	**–1.8**	**–1.9**	**–1.7**	**–1.6**

higher release height (z_r) shift the dispersal kernels to the right, toward longer dispersal distances with higher variance around the mean. Similar strong effects for v_t and z_r were also observed using a long-term seed-rain data in a tropical environment (Muller-Landau *et al.* 2008). Dispersal kernels can be separated into two types based on the absolute definition of LDD (>100 m): (i) Those that only describe short-distance dispersal and have a unimodal shape with an exponential slope at the far end; and (ii) those that include LDD and have a distinct tail at the far end. The slope of a power-law fit for the tail of these LDD dispersal kernels is less steep than the far end of the short-distance-only dispersal kernels. When LDD is significant, the magnitude of the slope reaches a minimum of 1.6 (Table 2). A conceptual divide, hereafter referred to as the 'LDD-divide' (Fig. 1), can be drawn between the short-distance-only kernels, where LDD is very unlikely, and the kernels in which slow v_t and high z_r enable some of the seeds to be uplifted above the highest point in the canopy (40.5 m) and experience LDD. In fact, the seed dispersal distance is well correlated with the maximal flight height if the seeds are ejected above the canopy (Fig. 2).

ASSUMPTION OF NO-INERTIA

In almost all cases, whether experiencing LDD or not, the virtual tracers dispersed farther than the natural seeds (Table 3). This is more pronounced with the fast-falling seeds (whose mean distance increased by about 15%) than with the slow-falling seeds, which are more susceptible to LDD (up to only about 5%). Ignoring inertia has similar effects on the variance of the dispersal distance, but has no significant effects on the LDD tail of the kernel (represented by the mean distance of the 0.01-percentile of the farthest-dispersing seeds).

ABSCISSION WIND SPEED

Figure 3 summarizes the results of the AWS experiment. It emphasizes that under the considered conditions, an AWS of 0.5 m s^{-1}, which is about the same magnitude as the standard deviation of the vertical wind (σ_w) has only a minor impact on the dispersal kernels in general, and LDD in particular. An

Table 3. Mean and variance of the dispersal distance (m) and the distance of the 0.01% farthest reaching seeds (the kernel's '0.01%-tail'), in natural seeds (N) and virtual tracers (VT) (columns) for combinations of v_t and z_r representing extreme dispersal kernels, i.e. no-LDD cases in the top four rows, and LDD-dominant cases in the lower three rows

		Mean		Variance		0.01%-tail distance	
v_t (m s^{-1})	z_r (m)	VT	N	VT	N	VT	N
1.89	18	5.61	4.81	8.56	6.46	13.99	12.47
	24	7.61	6.59	14.2	11.44	19.62	18.21
1.43	18	6.9	6.13	11.94	10.02	17.79	16.4
	24	9.72	8.79	21.08	18.4	24.69	23.78
1.43	39	22.09	21.27	111.21	106.16	896.37	980.97
1.1	39	35.13	33.99	3667.32	3200.52	1396.18	1207.04
0.67	39	92.5	87.95	47140.96	40367.83	2124.21	2259.96

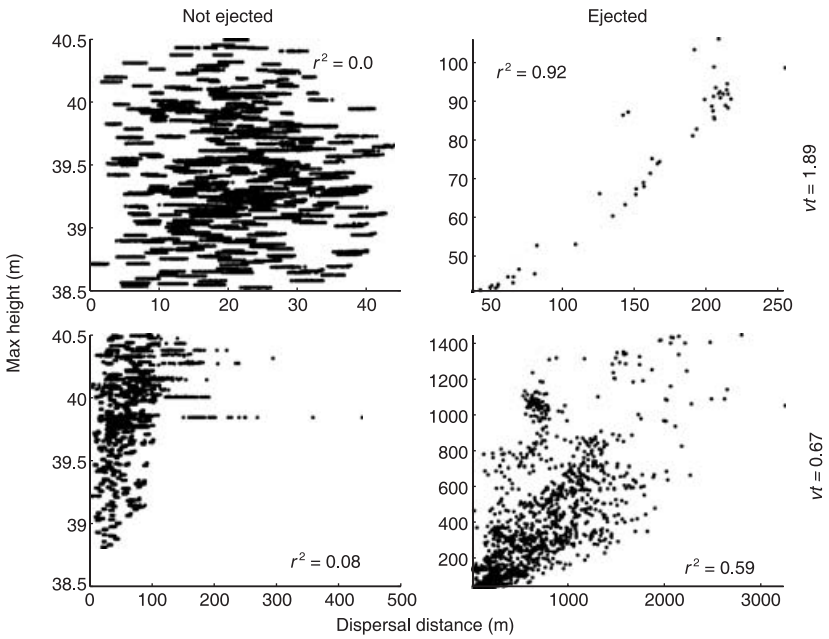

Fig. 2. Correlation between maximal height reached and dispersal distance. z_r = 39 m AGL in all panels. Ejected seeds are those that at some point of their flight reached the model grid layer above the tallest tree (40.5 m). The maximal height reached is correlated with farther dispersal distance only for ejected seeds.

AWS of 1 m s^{-1} (about twice σ_w) with optimal conditions for LDD (low v_t and high z_r) shows an increase of about 20% for the median dispersal distance, but appears to have no conclusive effect on the dispersal kernel tail.

TREE-SCALE CANOPY HETEROGENEITY

Table 4 summarizes the effects of canopy height (h_c) at the release point, which should not be confused with the seed release height (z_r). h_c has a significant effect on LDD, but does not consistently affect short-distance dispersal, expressed by the median dispersal distance. Low h_c increases the probability of uplift by promoting stronger and more frequent atmospheric mass ejection events in the lower parts of the canopy (illustrated in Fig. 4). Seeds not prone to LDD (high v_t and low z_r) are, therefore, not affected by the canopy-top height. However, seeds that have a better chance of being uplifted experience longer LDD when released from a location with a low h_c. This non-intuitive effect is apparent in the borderline cases where LDD is possible but extremely rare, such as for seeds with v_t = 0.67 m s^{-1} released from z_r = 24 m, and seeds with v_t = 1.1 or 1.43 m s^{-1} released from z_r = 39 m. Kernels of seeds with these release heights and terminal velocities have a distinct tail only for those seeds released from low canopies (i.e. h_c = 17 m and h_c = 25 m, Fig. 1, purple and light blue lines), kernels of seeds with the same v_t and z_r combinations but released from tall canopies (i.e. h_c = 30 m and h_c = 39 m, Fig. 1, green and red lines) do not display LDD.

Discussion

An upsurge in research interest in biological transport processes through the atmosphere (Nathan *et al.* 2005; Nathan 2006) is perhaps best exemplified by the recent advances in mechanistic modelling of seed dispersal by wind (Levin *et al.* 2003; Kuparinen 2006). Several simple mechanistic models introduced in the last two decades have been shown to match dispersal data measured at local scales (e.g. Okubo & Levin

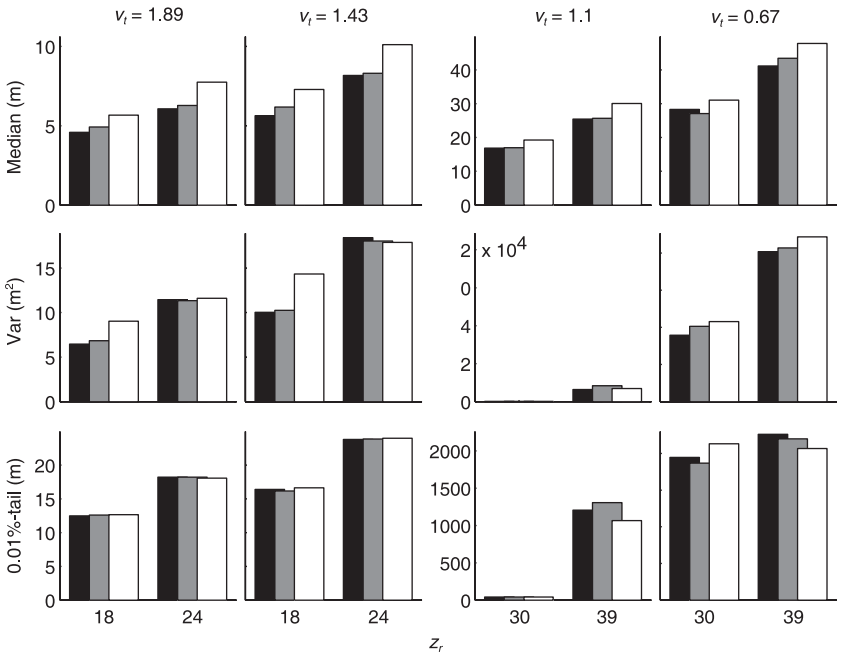

Fig. 3. Impacts of AWS on dispersal distance statistics. Black, grey and white bars represent AWS = 0, 0.5, and 1 m s^{-1}, respectively, h_c = 17 m in all cases. The left columns are for short-distance-only and the right columns are for LDD-dominant cases.

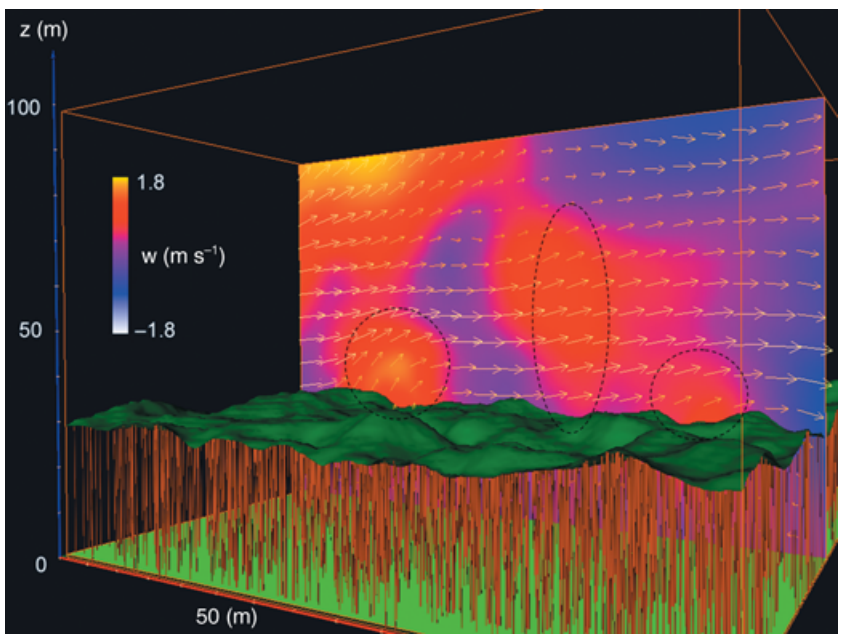

Fig. 4. Cross section (x–z) of wind velocities in a 200 × 200 × 100 m^3 sub-domain of the control simulation. Colours on the vertical plane indicate the vertical component of the wind, and arrows indicate the wind vector. Canopy tops contour is green and stems are brown. Three momentum ejections sites are highlighted with dashed contours, and occur where the canopy top is relatively low.

Table 4. Percentage of seeds that travelled more than 100 m, 0.01%-tail distance, and median dispersal distance (m) of seeds released from locations with different canopy heights (h_c, m) for different combinations of v_t and z_r (rows)

		% > 100 m		0.01%-tail distance		Median	
v_t (m s^{-1})	z_r (m)	h_c = 17	h_c = 39	h_c = 17	h_c = 39	h_c = 17	h_c = 39
1.89	39	0	0	38.73	37.38	15.00	11.05
1.43	39	0.08	0	980.97	59.19	19.30	16.11
1.1	39	1.65	0.60	1207.04	1508.56	25.46	21.98
0.67	39	10.6	9.51	2259.96	2139.50	41.15	36.10
0.67	30	4.59	1.37	1944.50	1966.08	28.33	23.94
0.67	24	0.94	0.11	1414.43	188.28	18.91	18.63
0.67	18	0.03	0	184.15	40.31	12.74	13.10

1989; Greene & Johnson 1995; Skarpaas *et al*. 2004), but have failed to fit or explain LDD (e.g. Greene & Johnson 1995; Nathan *et al*. 2001). These models were recently followed by two main modelling approaches, one based on local, high-resolution wind measurements (PAPPUS, Tackenberg 2003) and assumed to be planar homogeneous throughout the dispersal domain, the other coupling Eulerian closure techniques with Lagrangian simulations of particle trajectories (e.g. CELC, Nathan *et al*. 2002; Soons *et al*. 2004; Nathan & Katul 2005). These newer models performed well when compared to observed data and, by relaxing some unrealistic assumptions of their precedents, have provided new insights into the mechanisms underlying LDD. Despite this important progress, two main challenges in mechanistic modelling of seed dispersal by wind remained, leading to two opposing motivations guiding subsequent model development. On the one hand, high-resolution E–L models are computer-intensive and cannot be applied for long-term large-scale problems for which LDD plays a major role (Neilson *et al*. 2005; Trakhtenbrot *et al*. 2005). On the other hand, CELC and nearly all other advanced E–L models (e.g. Boehm & Aylor 2005; Kuparinen *et al*. 2007) neither relax nor examine several key simplifying assumptions such as landscape homogeneity, wind speed independent seed release, and perfect tracking of wind flow by seeds caused by the lack of inertial effects on the seed. Yet all these factors can be assumed to significantly affect the distance travelled by wind-dispersed seeds.

Research motivation to facilitate the application of mechanistic wind dispersal models to long-term population dynamics has recently yielded WALD, an analytical model derived from CELC with some additional simplifications of the underlying mechanisms (K05). WALD was shown to match empirical data well and to resolve the high computing demands of its precursors (K05; Skarpaas & Shea 2007). The opposing motivation to explore wind dispersal mechanisms in more depth has yielded RAFLES, the model introduced in the present paper. To our knowledge, RAFLES is the first LES-based E–L model capable of simulating seed dispersal by wind in 3D heterogeneous canopies. It is far more detailed than any previous mechanistic model of seed dispersal by wind and, as such, has considerably higher computational demands. Whereas such computational demands imply that RAFLES cannot be applied to predict long-term dispersal dynamics, its ability to simulate nonlinear processes and to relax and examine some major simplifications common to nearly all previous models, uniquely fulfills the important alternative motivation of using wind dispersal models to better understand the mechanisms underlying the dispersal process.

Interestingly, in spite of their conceptual difference, WALD and RAFLES converge to the same asymptotic behaviour for LDD in the case of lighter seeds (and high winds). WALD predicts an asymptotic power-law slope of –3/2 for the most favourable LDD conditions (seeds with low terminal velocity transported by strong winds). Dispersal kernels predicted by RAFLES depict a distinct LDD tail for slow-falling seeds released from higher points (Fig. 1, below the 'LDD divide'). The slower the fall velocity and the higher the release point, the more prevalent LDD becomes and the fitted power-law slope of the tail approaches the same asymptotic value of –3/2 (Table 2).

By virtue of its high resolution and detailed mechanistic approach, RAFLES explicitly incorporates physical processes that have only been parameterized or neglected in other models. The physical processes that are explicitly resolved in RAFLES include the effects of canopy structure on ABL dynamics and turbulence, wind speed conditioned seed release and seed inertia effects. It can simulate the mechanistic processes that account for the possible feedbacks between canopy structure, atmospheric dynamics and seed biology, occurring at different spatial scales. In the following sections, we discuss the key interactions underlying wind dispersal at two different spatial scales: those of the seed and the tree.

SEED SCALE

Abscission

The mechanical force that detaches the seed from the tree is generated by drag, acting in the direction of the air flow. Here, abscission was implemented as a threshold function of the instantaneous wind speed, which is a directionless scalar. But, abscission is only effective if it occurs in limited periods of time, characterized by infrequent (strong) wind gusts. Turbulence is characterized by coherent structures in the flow field (Raupach *et al*. 1996; Finnigan 2000; Watanabe 2004), which are generated near the canopy top by mechanical shear and/or buoyancy. These structures, or eddies, evolve while they are advected through the ABL. Seeds that are released by strong eddies, may then be transported by them. When the abscission process is biased toward strong eddies, 'riding' on the eddies will allow the seeds to be ejected above the canopy more often and disperse greater distances. By explicitly resolving the seed movement in deterministic eddy structures, RAFLES can test this mechanism. The low AWS used here, on the order of 1 SD of the vertical wind speed, (σ_w = 0.4 – 0.6 m s^{-1}, depending on the release height), has only minor effects on the dispersal kernels. The stronger AWS, about $2 \times \sigma_w$ affects the median dispersal distance but does not affect LDD. This finding nullifies our hypothesis as well as general expectations from wind tunnel experiments (Schippers & Jongejans 2005). It may be explained by the tendency of strong wind gusts to occur in both ejections (updrafts) and sweeps (downdrafts), generated by shear between the wind aloft and the slower air flow inside the canopy, and by convection. While the mean vertical wind is zero, sweeps are more common but weaker than ejections within the canopy (Kaimal & Finnigan 1994; Poggi *et al*. 2004). Therefore, in weak wind conditions as tested here, an AWS > 0 may result in more dispersal events during sweeps than during ejections. Setting AWS to a value higher than the maximum wind speed simulated in our numerical experiment would prevent the virtual release of these seeds. Of course, over the season that is relevant for seed dispersal, the likelihood of much stronger wind gusts than those simulated

here cannot be neglected. Clearly, it is the relationship between AWS and the frequency of such strong wind gusts that matters (Schippers & Jongejans 2005). An AWS of above 4 m s^{-1} was observed in two grassy species (Soons & Bullock 2008). Such a high value very close to the ground (the wind gets weaker close to the ground, following a logarithmic profile) indicates that AWS may be affecting dispersal at longer (days-season) time scales, yet our simulations suggest that as long as the AWS is contained within $2 \times \sigma_w$, it affects neither the mean nor the tail of the dispersal distribution.

Effects of Inertia

Neglecting inertia and treating dispersing seeds (or other particles in the atmosphere) as passive tracers is a common and convenient assumption, which simplifies the system in general, and its numerical modelling in particular. RAFLES represents some of the effects of inertia on seeds movements. By comparing the dispersal kernels of 'natural' seeds and passive tracers that are only subjected to gravity, one can 'bracket' the magnitude of the error introduced by neglecting inertia. Our simulations show that, at most, the mean dispersal distance is increased by 15% with the no-inertia assumption, but the probability of LDD is not significantly affected. It is important to emphasize that we have not exhausted this issue and that our conclusions may not hold for different species. For instance, seeds of some tropical tree and liana species such as the tropical vine *Alsomitra macrocarpa* (Azuma & Okuno 1987) are heavy yet have relatively low terminal velocity and modelling their movement may exhibit a much stronger sensitivity to inertia. The aerodynamic shapes of some seed species can lead to strong nonlinearity in the relationship between the drag coefficient and *Re*, and generate a stronger effect on the simulated dispersal path than found in this study.

TREE-SCALE

Tree-scale heterogeneity refers here to variation in leaf area density and tree-top height from tree to tree of a common canopy. To date, most models assumed horizontal homogeneity of the surface. Unlike RAFLES, other mechanistic and spatially explicit E–L models that use turbulence statistics cannot resolve the effects of individual trees on eddy structures. Therefore, they are unable to resolve the interactions between canopy structure and dispersal. Yet B07 have shown that tree-scale heterogeneity affects the spatial occurrences of momentum ejections and, to a lesser extent, sweeps. Strong updrafts, which are associated with momentum ejection events, are anchored in areas of the canopy where the trees are short and leaf area density is low (Fig. 4). Based on these results, we hypothesized that the change in turbulence structure that is caused by tree-scale canopy structures will also affect dispersal. The simulations presented here show that, indeed, when seeds are released from an area with increased momentum ejection activity, the probability that they will encounter a strong updraft and escape the canopy is higher. Then, they also travel larger distances (Fig. 2) because higher above the surface, the stronger horizontal wind can carry the seeds further away during the time period that it takes for such seeds to fall to the ground. This mechanism is particularly effective in cases where LDD is possible but extremely rare (Fig. 1, Tables 2 and 4).

Conclusions and future directions

Using RAFLES coupled with an E–L seed dispersal module, we have studied how the interactions among 3D canopy structure, wind (turbulence), and seed (aerodynamic) properties impact dispersal kernels. In particular, we have explored the importance of canopy heterogeneity, seed inertia and wind speed dependent seed abscission in a realistic canopy submitted to observed meteorological conditions in Durham, NC, USA.

The high resolution of RAFLES and its highly detailed mechanistic approach led to three main novel insights on the effects of small-scale turbulent eddies on seed dispersal. First, our simulations demonstrate that for the set of atmospheric conditions, seed properties and abscission conditions tested here, AWS of up to twice the standard deviation of the vertical wind affects mostly SDD and not LDD. Second, we show that the uplifting probability and LDD are not sensitive to the assumption of no inertia, at least within the assumption of a constant C_d. Furthermore, the incorporation of seed inertia and drag forces induce a relatively small (< 15%) change in the predicted mean dispersal distance. This is surprising because seeds of most wind-dispersed tree species, like those included in our study, are relatively heavy and thus the commonly-held assumption of no inertia taken thus far by all seed dispersal models has been questioned by scholars experienced with modelling of pollen, dust and other very small particles, for which neglecting inertia is soundly based on theory and measurements. Third, we found that seeds released from relatively short trees not overcast by taller canopy trees, are more likely to encounter strong updrafts and higher probabilities of being ejected above the canopy and experiencing LDD than trees in other parts of the forest. This non-intuitive novel finding concretely demonstrate the power of RAFLES in elucidating the wind dispersal mechanisms in non-homogeneous landscapes. It suggests that particular (diagnosable) sites within a heterogeneous forest are 'hotspots' of LDD. Thereby local structures, such as a leafless deciduous tree within an evergreen canopy, or natural and anthropogenic disturbances such as selective logging, parasite infestation, wind damage, and local fire that change the canopy structure at the tree-scale, can affect long-term large-scale tree population dynamics.

RAFLES is too demanding of computer resources to be used for explicit seed dispersal predictions at long time-scales and/or large domains. Its computational demands prevented us from testing other interesting cases, which would be quite valuable for thoroughly understanding the multiple complex processes involved in seed dispersal by wind. For example, it seems that it would be quite valuable to examine how stormy weather, coupled with high AWS, affects LDD. Indeed, one

could speculate that with high AWS, trees can 'wait' for the less frequent events (e.g. thunderstorms) characterized by exceptionally strong winds favourable for LDD. Other major unanswered questions most suitable for future model exploration relate to how canopy gaps of different shape and size affect airflow and seed dispersal (release, flight and deposition) patterns. Seed dispersal from trees at the forest edge is another interesting complexity that could be investigated. Combined with improved methods of seed-rain observation and interpretation, such as long-term seed trapping and genetic methods (e.g. Jones & Muller-Landau 2008) insights gained by such numerical studies may be used to develop and test parameterizations of less complex models. Finally, the scope of questions can be extended to those relevant to the study of wind dispersal of other life forms in heterogeneous vegetation formations other than forests.

Acknowledgements

We wish to thank Charles Canham and two anonymous referees, Massimo Cassiani for help in implementation of the dispersal scheme, Mario Siquiera and Jehn-Yih Juang for providing the eddy flux observations, Ram Oren, Heather McCarthy, Chris Oishi, Hyun-Seuk Kim, Michael Wolosin and Mathieu Therezien for canopy data, Stefano Manzoni, Andrey Khlystov, Mark Wiesner and John Albertson for advice on seed representation and particle interception by the canopy, Kathy Walko and Heidi Holder for comments on the manuscript, Martin Otte and Ron Stubbs for IT support and Suvi Thomas, Inés Ibáñez and Shannon LaDeau for their help with the release experiments at Duke Forest. This study was funded in part by NOAA grant #NA030AR4310150 and NSF grants #IBN-9981620, #DEB-0453665, and #EAR-0628342 and USDA CSREES grant # 2005-03804. The Duke Forest turbulence data were supported by the US Department of Energy (DOE) through the Office of Biological and Environmental Research (BER) Terrestrial Carbon Processes (TCP) program (Grants # 10509-0152, DE-FG02-00ER53015, and DE-FG02-95ER62083). RN was supported by the Israeli Science Foundation (ISF 474/02 and ISF-FIRST 1316/05), the Simon and Ethel Flegg Fellowship, and the Friedrich Wilhelm Bessel Research Award of the Humboldt Foundation. GB was supported in part by the John and Elaine French fellowship of the Harvard University Center for the Environment.

References

Andersen, M. (1991) Mechanistic models for the seed shadows of wind-dispersed plants. *American Naturalist*, **137**, 476–497.

Augspurger, C.K. & Franson, S.E. (1988) Input of wind-dispersed seeds into light-gaps and forest sites in a neotropical forest. *Journal of Tropical Ecology*, **4**, 239–252.

Avissar, R. & Schmidt, T. (1998) An evaluation of the scale at which ground-surface heat flux patchiness affects the convective boundary layer using large-eddy simulations. *Journal of the Atmospheric Sciences*, **55**, 2666–2689.

Azuma, A. & Okuno, Y. (1987) Flight of a samara, *Alsomitra macrocarpa*. *Journal of Theoretical Biology*, **129**, 263–274.

Boehm, M.T. & Aylor, D.E. (2005) Lagrangian stochastic modeling of heavy particle transport in the convective boundary layer. *Atmospheric Environment*, **39**, 4841–4850.

Bohrer, G. (2007) *Large Eddy Simulations of Forest Canopies for Determination of Biological Dispersal by Wind*. Duke University, Durham, NC.

Bohrer, G., Wolosin, M., Brady, R. & Avissar, R. (2007) A Virtual Canopy Generator (V-CaGe) for modeling complex heterogeneous forest canopies at high resolution *Tellus Series B-Chemical and Physical Meteorology*, **59**, 566–576.

Clark, J.S., Lewis, M. & Horvath, L. (2001) Invasion by extremes: population spread with variation in dispersal and reproduction. *American Naturalist*, **157**, 537–554.

Clark, J.S., Silman, M., Kern, R., Macklin, E. & HilleRisLambers, J. (1999) Seed dispersal near and far: patterns across temperate and tropical forests. *Ecology*, **80**, 1475–1494.

Csanady, G.T. (1963) Turbulent diffusion of heavy particles in the atmosphere. *Journal of the Atmospheric Sciences*, **20**, 201–208.

Dalling, J.W., Muller-Landau, H.C., Wright, S.J. & Hubbell, S.P. (2002) Role of dispersal in the recruitment limitation of neotropical pioneer species. *Journal of Ecology*, **90**, 714–727.

Finnigan, J. (2000) Turbulence in plant canopies. *Annual Review of Fluid Mechanics*, **32**, 519–571.

Forget, P.M., Lambert, J.E. & Hulme, P.E., eds. (2004) *Seed Fate: Predation, Dispersal and Seedling Establishment*, p. 426. CAB International, Wallingford, UK.

Greene, D.F. & Johnson, E.A. (1989) A model of wind dispersal of winged or plumed seeds. *Ecology*, **70**, 339–347.

Greene, D.F. & Johnson, E.A. (1990) The dispersal of winged fruits and seeds differing in autorotative behavior. *Canadian Journal of Botany-Revue Canadienne De Botanique*, **68**, 2693–2697.

Greene, D.F. & Johnson, E.A. (1992) Fruit abscission in *Acer saccharinum* with reference to seed dispersal. *Canadian Journal of Botany-Revue Canadienne De Botanique*, **70**, 2277–2283.

Greene, D.F. & Johnson, E.A. (1995) Long-distance wind dispersal of tree seeds. *Canadian Journal of Botany-Revue Canadienne De Botanique*, **73**, 1036–1045.

Higgins, S.I. & Cain, M.L. (2002) Spatially realistic plant metapopulation models and the colonization-competition trade-off. *Journal of Ecology*, **90**, 616–626.

Horn, H.S., Nathan, R. & Kaplan, S.R. (2001) Long-distance dispersal of tree seeds by wind. *Ecological Research*, **16**, 877–885.

Jones, F.A. & Muller-Landau, H.C. (2008) Measuring long distance seed dispersal in complex natural environments: an evaluation and integration of classical and genetic methods. *Journal of Ecology*, **96**, 642–652.

Kaimal, J.C. & Finnigan, J.J. (1994) *Atmospheric Boundary Layer Flows: Their Structure and Measurement*. Oxford University Press, New York, NY.

Katul, G.G. & Albertson, J.D. (1998) An investigation of higher-order closure models for a forested canopy. *Boundary-Layer Meteorology*, **89**, 47–74.

Katul, G.G. & Chang, W.H. (1999) Principal length scales in second-order closure models for canopy turbulence. *Journal of Applied Meteorology*, **38**, 1631–1643.

Katul, G.G., Porporato, A., Nathan, R., Siqueira, M., Soons, M.B., Poggi, D., Horn, H.S. & Levin, S.A. (2005) Mechanistic analytical models for long-distance seed dispersal by wind. *American Naturalist*, **166**, 368–381.

Kim, S.-W., Moeng, C.-H., Weil, J.C. & Barth, M.C. (2005) Lagrangian particle dispersion modeling of the fumigation process using large-eddy simulation. *Journal of the Atmospheric Sciences*, **62**, 1932–1946.

Kot, M., Lewis, M.A. & vandenDriessche, P. (1996) Dispersal data and the spread of invading organisms. *Ecology*, **77**, 2027–2042.

Kuparinen, A. (2006) Mechanistic models for wind dispersal. *Trends in Plant Science*, **11**, 296–301.

Kuparinen, A., Markkanen, T., Riikonen, H. & Vesala, T. (2007) Modeling air-mediated dispersal of spores, pollen and seeds in forested areas. *Ecological Modelling*, **208**, 177–188

Lefsky, M.A., Cohen, W.B., Parker, G.G. & Harding, D.J. (2002) Lidar remote sensing for ecosystem studies. *BioScience*, **52**, 19–30.

Levey, D.J., Silva, W.R. & Galetti, M., eds. (2002) *Seed Dispersal and Frugivory: Ecology, Evolution and Conservation*, p. 500. CAB International, Wallingford, UK.

Levin, S.A., Muller-Landau, H.C., Nathan, R. & Chave, J. (2003) The ecology and evolution of seed dispersal: a theoretical perspective. *Annual Review of Ecology Evolution and Systematics*, **34**, 575–604.

Levine, J.M. & Murrell, D.J. (2003) The community-level consequences of seed dispersal patterns. *Annual Review of Ecology Evolution and Systematics*, **34**, 549–574.

Lien, R.C. & D'Asaro, E.A. (2002) The Kolmogorov constant for the Lagrangian velocity spectrum and structure function. *Physics of Fluids*, **14**, 4456–4459.

McCarthy, H.R., Oren, R., Finzi, A.C., Ellsworth, D.S., Kim, H.-S., Johnsen, K.H. & Millar, B. (2007) Temporal dynamics and spatial variability in the enhancement of canopy leaf area under elevated atmospheric CO_2. *Global Change Biology*, **13**, 2479–2497.

Muller-Landau, H.C., Wright, S.J., Calderón, O., Condit, R. & Hubbell, S.P. (2008) Interspecific variation in primary seed dispersal in a tropical forest. *Journal of Ecology*, **96**, 653–667.

Nathan, R. (2005) Long-distance dispersal research: building a network of yellow brick roads. *Diversity and Distributions*, **11**, 125–130.

Nathan, R. (2006) Long-distance dispersal of plants. *Science*, **313**, 786–788.

Nathan, R. & Katul, G.G. (2005) Foliage shedding in deciduous forests lifts up long-distance seed dispersal by wind. *Proceedings of the National Academy of Sciences of the United States of America*, **102**, 8251–8256.

Nathan, R. & Muller-Landau, H.C. (2000) Spatial patterns of seed dispersal, their determinants and consequences for recruitment. *Trends in Ecology and Evolution*, **15**, 278–285.

Nathan, R., Katul, G.G., Horn, H.S., Thomas, S.M., Oren, R., Avissar, R., Pacala, S.W. & Levin, S.A. (2002) Mechanisms of long-distance dispersal of seeds by wind. *Nature*, **418**, 409–413.
Nathan, R., Perry, G., Cronin, J.T., Strand, A.E. & Cain, M.L. (2003) Methods for estimating long-distance dispersal. *Oikos*, **103**, 261–273.
Nathan, R., Safriel, U.N. & Noy-Meir, I. (2001) Field validation and sensitivity analysis of a mechanistic model for tree seed dispersal by wind. *Ecology*, **82**, 374–388.
Nathan, R., Sapir, N., Trakhtenbrot, A., Katul, G.G., Bohrer, G., Otte, M., Avissar, R., Soons, M.B., Horn, H.S., Wikelski, M. & Levin, S.A. (2005) Long-distance biological transport processes through the air: can nature's complexity be unfolded *in silico*? *Diversity and Distributions*, **11**, 131–137.
Neilson, R.P., Pitelka, L.F., Solomon, A.M., Nathan, R., Midgley, G.F., Fragoso, J.M.V., Lischke, H. & Thompson, K. (2005) Forecasting regional to global plant migration in response to climate change. *BioScience*, **55**, 749–759.
Nuttle, T. & Haefner, J.W. (2005) Seed dispersal in heterogeneous environments: bridging the gap between mechanistic dispersal and forest dynamics models. *American Naturalist*, **165**, 336–349.
Okubo, A. & Levin, S.A. (1989) A theoretical framework for data-analysis of wind dispersal of seeds and pollen. *Ecology*, **70**, 329–338.
Poggi, D., Katul, G.G. & Albertson, J. (2006) Scalar dispersion within a model canopy: measurements and three-dimensional Lagrangian models. *Advances in Water Resources*, **29**, 326–335.
Poggi, D., Porporato, A., Ridolfi, L., Albertson, J.D. & Katul, G.G. (2004) The effect of vegetation density on canopy sub-layer turbulence. *Boundary-Layer Meteorology*, **111**, 565–587.
Pounden, E., Greene, D.F., Quesada, M. & Contreras Sánchez, J.M. (2008) The effect of collisions with vegetation elements on the dispersal of winged and plumed seeds. *Journal of Ecology*, **96**, 591–598.
Raupach, M.R., Finnigan, J.J. & Brunet, Y. (1996) Coherent eddies and turbulence in vegetation canopies: the mixing-layer analogy. *Boundary-Layer Meteorology*, **78**, 351–382.
Raupach, M.R., Woods, N., Dorr, G., Leys, J.F. & Cleugh, H.A. (2001) The entrapment of particles by windbreaks. *Atmospheric Environment*, **35**, 3373–3383.
Reynolds, A.M. & Lo Iacono, G. (2004) On the simulation of particle trajectories in turbulent flows. *Physics of Fluids*, **16**, 4353–4358.
Sawford, B.L. & Guest, F.M. (1991) Lagrangian statistical simulation of the turbulent motion of heavy-particles. *Boundary-Layer Meteorology*, **54**, 147–166.
Schippers, P. & Jongejans, E. (2005) Release thresholds strongly determine the range of seed dispersal by wind. *Ecological Modelling*, **185**, 93–103.
Schurr, F.M., Steinitz, O. & Nathan, R. (2008) Plant fecundity and seed dispersal in spatially heterogeneous environments: models, mechanisms and estimation. *Journal of Ecology*, **96**, 628–641.
Skarpaas, O. & Shea, K. (2007) Dispersal patterns, dispersal mechanisms, and invasion wave speeds for invasive thistles. *American Naturalist*, **170**, 421–430.
Skarpaas, O., Stabbetorp, O.E., Rønning, I. & Svennungsen, T.O. (2004) How far can a hawk's beard fly? Measuring and modelling the dispersal of *Crepis praemorsa*. *Journal of Ecology*, **92**, 747–757.
Soons, M.B. & Bullock, J.M. (2008) Non-random seed abscission, long-distance wind dispersal, and plant migration rates. *Journal of Ecology*, **96**, 581–590.
Soons, M.B., Heil, G.W., Nathan, R. & Katul, G.G. (2004) Determinants of long-distance seed dispersal by wind in grasslands. *Ecology*, **85**, 3056–3068.
Tackenberg, O. (2003) Modeling long-distance dispersal of plant diaspores by wind. *Ecological Monographs*, **73**, 173–189.
Thomson, D. (1987) Criteria for the selection of stochastic-models of particle trajectories in turbulent flows. *Journal of Fluid Mechanics*, **180**, 529–556.
Trakhtenbrot, A., Nathan, R., Perry, G. & Richardson, D.M. (2005) The importance of long-distance dispersal in biodiversity conservation. *Diversity and Distributions*, **11**, 173–181.
Volis, S., Bohrer, G., Oostermeijer, G. & Van Tienderen, P. (2005) Regional consequences of local population demography and genetics in relation to habitat management in *Gentiana pneumonanthe*. *Conservation Biology*, **19**, 357–367.
Walko, R.L., Tremback, C.J. & Bell, M.J. (2001). *HYPACT-Hybrid Particle and Concentration Transport Model, Version 1.2.0, User's Guide*. ASTER Division, Mission Research Corporation, Fort Collins, CO.
Watanabe, T. (2004) Large-eddy simulation of coherent turbulence structures associated with scalar ramps over plant canopies. *Boundary-Layer Meteorology*, **112**, 307–341.
Weil, J.C., Sullivan, P.P. & Moeng, C.H. (2004) The use of large-eddy simulations in Lagrangian particle dispersion models. *Journal of the Atmospheric Sciences*, **61**, 2877–2887.
Weishampel, J.F., Blair, J.B., Knox, R.G., Dubayah, R. & Clark, D.B. (2000) Volumetric lidar return patterns from an old-growth tropical rainforest canopy. *International Journal of Remote Sensing*, **21**, 409–415.
Williams, C.G., LaDeau, S.L., Oren, R. & Katul, G.G. (2006) Modeling seed dispersal distances: Implications for transgenic *Pinus taeda*. *Ecological Applications*, **16**, 117–124.
Wilson, J.R.U., Richardson, D.M., Rouget, M., Proches, S., Amis, M.A., Henderson, L. & Thuiller, W. (2007) Residence time and potential range: crucial considerations in modelling plant invasions. *Diversity and Distributions*, **13**, 11–22.
Yee, E. & Wilson, J.D. (2007) Instability in Lagrangian stochastic trajectory models, and a method for its cure. *Boundary-Layer Meteorology*, **122**, 243–261.

Received 2 August 2007; accepted 19 February 2008
Handling Editor: Charles Canham

Supplementary material

The following supplementary material is available for this article:

Appendix S1 RAFLES formulation, initialization and forcing.

Appendix S2 RAFLES evaluation.

This material is available as part of the online article from: http://www.blackwell-synergy.com/doi/abs/10.1111/j.1365-2745.2008.01368.x
(This link will take you to the article abstract).

Please note: Blackwell Publishing is not responsible for the content or functionality of any supplementary materials supplied by the authors. Any queries (other than missing material) should be directed to the corresponding author for the article.

Appendix S1. RAFLES formulation, initialization and forcing.

RAFLES solves the set of compressible, filtered Navier-Stokes equations written in quasi-Boussinesq form. The filtering is the result of discretization of the governing equations on grid-mesh volumes. All the variables are decomposed into two components $\varphi = \overline{\varphi} + \varphi'$ where $\overline{\varphi}$ is the resolved, grid averaged component, and φ' is the perturbation from this mean, i.e., the sub-grid scale (SGS) perturbation defined such that $\overline{\varphi'} = 0$. For numerical considerations, some variables are decomposed into a horizontally homogeneous, time constant, reference state, marked by a subscript "*0*", and a heterogeneous time-variable perturbation, marked by a subscript "*r*", i.e. $\varphi = \varphi_r + \varphi_0$. In this formulation pressure is expressed in terms of the Exner function, defined as $\pi = c_p \left(p / p_{00} \right)^{R_d / c_p} = c_p T / \theta$, where c_p is the specific heat of air, R_d is the gas constant, $p_{00} = 10^5$ [Pa] is approximately the standard sea-level pressure, T is air temperature, and θ is potential temperature. The model reference state is hydrostatically balanced according to $\partial \pi_0 / \partial x_3 = -g / \theta_{v0}$, where g is gravity and θ_v is virtual potential temperature.

Notation – Einstein notation for vector equations is used throughout this paper. A full description of this notation is provided in many textbooks (e.g., Stull, 1988), and only the basic rule is given here. Let V_i represent a generic velocity vector, with integer indices that can each take on the values 1, 2, or 3. Accordingly, $V_1 = u$, $V_2 = v$, and $V_3 = w$ that is, in the longitudinal, latitudinal and vertical direction, respectively). X_i represents distance in a Cartesian coordinate system where $X_1 = x$, $X_2 = y$, and $X_3 = z$.

Governing equations – The prognostic equation for resolved-scale velocity is

$$\frac{\partial \overline{u_i}}{\partial t} + \frac{1}{\rho_0}\left[-\overline{u_i}\frac{\partial\left(\rho_0 \overline{u_j}\right)}{\partial x_j} + \frac{\partial\left(\rho_0 \overline{u_i}\ \overline{u_j}\right)}{\partial x_j} + \frac{\partial\left(\rho_0 \overline{u_i' u_j'}\right)}{\partial x_j} \right] = \delta_{i3} g \frac{\overline{\theta_{vr}}}{\theta_{v0}} - 2\varepsilon_{ijk}\Omega_j\left(\overline{u_k} - u_{g_k}\right) - \theta_0\left(\frac{\partial \overline{\pi_r}}{\partial x_i}\right) + F\left(\overline{u_i}\right) + D_i\left(\overline{\mathbf{V}}\right) \tag{A.1}$$

where u_i is wind velocity, ρ is air density, t is time, δ is the Kronecker delta, Ω is the angular velocity vector of the earth, u_{gi} is geostrophic wind, $D_i\left(\overline{\mathbf{V}}\right)$ represents the component of the canopy drag force that is a function of the resolved scale velocity, and $F\left(\overline{u_i}\right)$ represents the sum per unit mass of horizontal wind forcing through the domain, which is comprised of Rayleigh friction and a Newtonian nudging term that maintains a mean mesoscale horizontal wind profile.

The prognostic equation for the Exner function is derived from the continuity of energy (Klemp & Wilhelmson, 1978):

$$\frac{\partial \overline{\pi}}{\partial t} = \frac{-{c_{sp}}^2}{\rho_0 {\theta_0}^2}\frac{\partial\left(\rho_0 \theta_0 \overline{u_j}\right)}{\partial x_j} \tag{A.2}$$

where c_{sp} is the effective speed of sound, which for numerical stability has been reduced relative to the physical speed of sound.

The equation for conservation of energy at the resolved scale is

$$\frac{\partial \overline{\theta}}{\partial t} = \frac{1}{\rho_{a0}} \left[\frac{\overline{\theta} \partial \left(\rho_0 \overline{u_j} \right)}{\partial x_j} - \frac{\partial \left(\rho_0 \overline{u_j} \overline{\theta} \right)}{\partial x_j} - \frac{\partial \left(\rho_0 \overline{u_j' \theta'} \right)}{\partial x_j} \right] + S_\theta \qquad \text{(A.3)}$$

where S_θ is the sum of sources and sinks of heat within the mesh volume. RAFLES also uses similar formulation for conservation of vapor and other scalars.

The prognostic equation for the (filtered) sub-grid scale (SGS) turbulence kinetic energy (TKE), $\bar{e} = u_i'^2 / 2$ (Deardorff, 1980):

$$\begin{aligned} &\frac{\partial \bar{e}}{\partial t} + \frac{\partial \left(\rho_0 \overline{u_j} \bar{e} \right)}{\rho_0 \partial x_j} - \frac{\bar{e}}{\rho_0} \frac{\partial \left(\rho_0 \overline{u_j} \right)}{\partial x_j} = \\ &\frac{g}{\overline{\theta_v}} \overline{w' \theta_v'} - \overline{u_i' u_j'} \frac{\partial \overline{u_i}}{\partial x_j} - \frac{\partial}{\partial x_i} \left(\overline{u_i' \left(E + \frac{p'}{\overline{\rho}} \right)} \right) - D_i \frac{\bar{e}}{\overline{u_i}} - \varepsilon \end{aligned} \qquad \text{(A.4)}$$

where E is the total TKE, $D_i \bar{e} / \overline{u_i}$ is the canopy drag on SGS motion and ε is turbulence dissipation.

The dissipation and the covariance of the SGS terms (e.g., $\overline{u_i' u_j'}$, $\overline{w' \theta_v'}$) are parameterized based on Deardorff (1980), with an additional Bhushan and Warsi (2005) backscatter for momentum. The generation of TKE by shear can be approximated by

$$\overline{u_i' u_j'} = -K_m \left(\frac{\partial \overline{u_i}}{\partial x_j} + \frac{\partial \overline{u_j}}{\partial x_i} \right) + \frac{2}{3} \delta_{ij} \bar{e} + \alpha_1 l_g^{\,2} \left(\frac{\partial \overline{u_i}}{\partial x_k} \frac{\partial \overline{u_j}}{\partial x_k} \right) - \alpha_2 l_g^{\,2} \left(\frac{\partial \overline{u_k}}{\partial x_i} \frac{\partial \overline{u_k}}{\partial x_j} \right) \qquad \text{(A.5)}$$

where $l_g = \left(2.25 \Delta x \Delta y \Delta z\right)^{1/3}$ is an empirical length scale that characterizes the mesh size (Patton, 1997), Δx, Δy, and Δz are the spatial grid spacing, $\alpha_1 = 1/12$ and $\alpha_2 = 0.0336$ are backscatter coefficients (Bhushan & Warsi, 2005), and K_m is the K-theory turbulence diffusivity for momentum. The transport of TKE can be approximated by

$$\overline{u_i' \left(E + \frac{p'}{\bar{\rho}} \right)} = -2K_m \frac{\partial \bar{e}}{\partial x_i} \qquad \text{(A.6)}$$

Scalar flux (including moisture) is approximated by

$$\overline{u_i' \chi'} = -K_h \left(\frac{\partial \overline{\chi}}{\partial x_i} \right) \qquad \text{(A.7)}$$

The vertical flux of virtual temperature is approximated by

$$\overline{w' \theta_v'} = -K_h \left(A \frac{\partial \overline{\theta_l}}{\partial z} + B \bar{\theta} \frac{\partial \bar{q}}{\partial z} \right) \qquad \text{(A.8)}$$

where θ, θ_v and θ_l are the potential, virtual potential, and potential water content temperatures; $\bar{q}$ is specific humidity; *A* and *B* are empirical functions defined as follows:

$$A = \begin{cases} 1 + 0.61\bar{q} & \text{unsaturated air} \\ 1 + 0.61\bar{q} - A_q & \text{saturated air} \end{cases}$$
$$B = \begin{cases} 0.61 & \text{unsaturated air} \\ \dfrac{c_v}{c_p \bar{T}} - 1 & \text{saturated air} \end{cases} \qquad \text{(A.9)}$$

where A_q is a correction for saturated air expressed as:

$$A_q = 0.622 \frac{c_v \overline{q_s}}{R_d \bar{T}} \times \left(\frac{c_v \left(1 + 0.61\bar{q}\right)}{c_p \bar{T}} - 1.61 \right) \times \left(1 + \frac{0.622 c_v^2 \overline{q_s}}{R_d c_p \bar{T}^2} \right)^{-1} \qquad \text{(A.10)}$$

$\overline{q_s}$ is specific humidity at saturation, and c_v is latent heat of vaporization. K_m and K_h approximated as:

$$K_m = 0.1 l_\varepsilon \bar{e}^{1/2}$$
$$K_h = K_m \left(1 + 2\frac{l_\varepsilon}{l_g}\right) \qquad \text{(A.11)}$$

where l_g and l_ε are empirical length scales for mesh size and dissipation, respectively:

$$l_g = \left[(1.5\Delta x)(1.5\Delta y)\Delta z \right]^{2/3}$$

$$l_\varepsilon = \begin{cases} l_g & \text{Stable ABL} \\ \min\left(l_g, 0.76\overline{e}^{1/2} \left(\dfrac{g}{\overline{\theta}_v} \dfrac{\partial \overline{\theta}}{\partial z} \right)^{-1/2} \right) & \text{Convective ABL} \end{cases} \tag{A.12}$$

Dissipation is approximated by

$$\varepsilon = \frac{\left(0.19 + \dfrac{0.51 l_\varepsilon}{l_g} \right) \overline{e}^{\frac{3}{2}}}{3 l_\varepsilon} \tag{A.13}$$

Initialization and forcing - Surface sensible and latent heat fluxes were derived from eddy-covariance observations at the Duke Forest meteorological tower. RAFLES was initialized with horizontally homogeneous atmospheric conditions (i.e., pressure, horizontal winds, temperature and humidity). The atmospheric conditions were produced with the Regional Atmospheric Modeling System (RAMS), which was forced with local radiosonde observations (see http://raob.fsl.noaa.gov/) and simulated the region around the Duke Forest at a horizontal resolution of 1 x 1 km^2. The horizontal winds were also used to force the mean horizontal wind above 100 m in RAFLES. The parameters defining the canopy and the mean canopy-top atmospheric conditions in both the control and homogeneous simulations are presented in Table A1.1. Vertical profiles of the simulated horizontal mean wind speed, standard deviation of vertical velocity, and potential virtual temperature from ground level up to 200 m above ground level (AGL) are presented in Figure A1.1.

Simulation time setup and seed release – The first 2 hours and 28 minutes of the model simulation are exactly the same as in (Bohrer, 2007). This initialization period is needed to dissipate the influence of the initial conditions and to allow turbulence to fully develop. However, following this initialization period, separate model runs were conducted due to the introduction of the E-L module. The model time step was 0.02 second. Seeds were virtually released only after the initialization period was completed. The virtual seeds were released at 40 locations as schematically illustrated in figure A.1.2. The simulation was run an additional seven minutes after the last release to allow nearly all seeds to settle. Seeds were considered settled when they first reached the forest floor. The model did not account for secondary dispersal due to re-suspension of settled seeds.

References

Bhushan, S. & Warsi, Z.U.A. (2005) Large eddy simulation of turbulent channel flow using an algebraic model. International Journal for Numerical Methods in Fluids, 49, 489-519.

Bohrer, G. (2007) Large eddy simulations of forest canopies for determination of biological dispersal by wind, Duke University, Durham, NC.

Deardorff, J.W. (1980) Stratocumulus-capped mixed layers derived from a 3-dimensional model. Boundary-Layer Meteorology, 18, 495-527.

Klemp, J.B. & Wilhelmson, R.B. (1978) Simulation of 3-dimensional convective storm dynamics. Journal of the Atmospheric Sciences, 35, 1070-1096.

Patton, E.G. (1997) Large-eddy simulation of turbulent flow above and within a plant canopy. Ph.D., University of California Davis, Davis.

Stull, R.B. (1988) An introduction to boundary layer meteorology. Kluwer Academic, Dordrecht, The Nederlands.

Atmosphere/canopy parameter	Control	Homogeneous
Canopy height [m]	24.06 (3.79)	24.06 (0)
LAI [m^2/m^2]	2.95 (0.26)	2.95 (0)
Bowen ratio	1.25 (0.16)	1.25 (0)
Length scale of heterogeneity [m]	6.53	∞
Surface flux [w/m^2]	286.27	291.55
Longitudinal wind [m/s]	0.83	0.64
u^* [m/s]	0.30	0.25
$\sigma_{\bar{w}}$ [m^2/s^2]	0.512	0.514
ABL stability parameter (ε)	-4.80	-6.54
ABL height [m]	680	680

Table A1.1. Mean and standard deviation (in parenthesis) of canopy spatial properties, and spatial and temporal mean (30 minutes) canopy-top atmospheric properties.

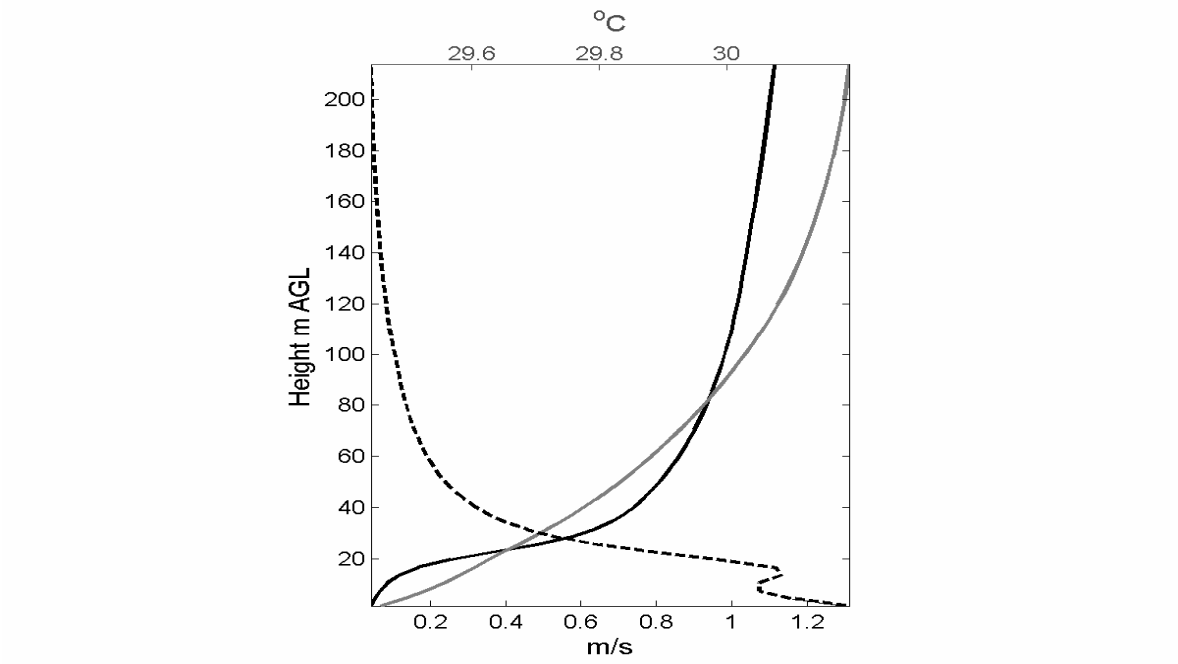

Figure A1.1 Simulated mean vertical profiles of the horizontal wind speed (black solid line, m/s), standard deviation of vertical velocity (gray solid line, m/s), and potential virtual temperature (dashed line, °C).

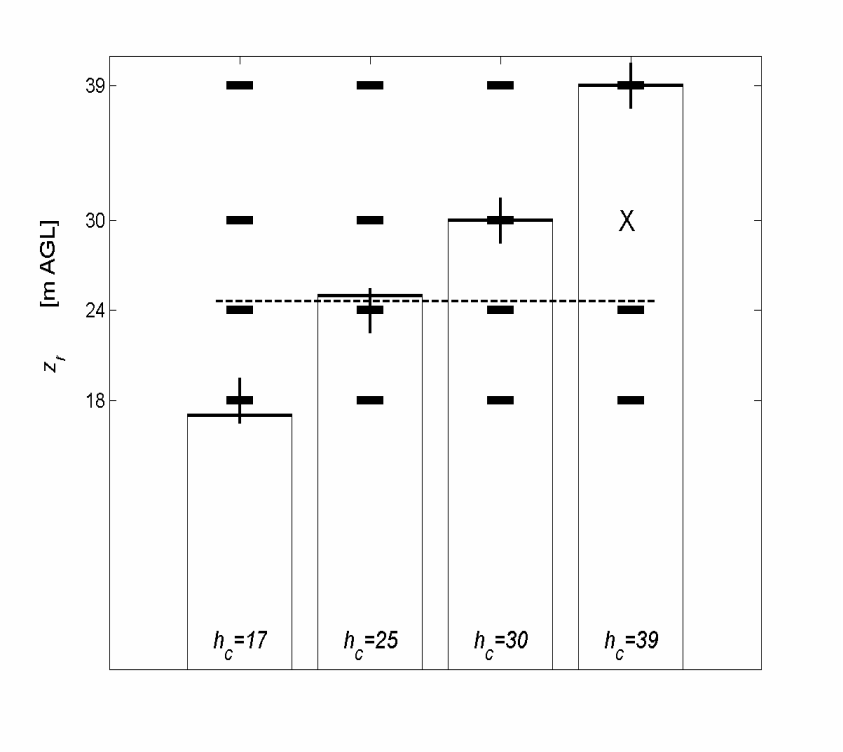

Figure A1.2. Columns indicate canopy height (h_c, in m), horizontal dashes indicate release heights (z_r), vertical bars indicate the numerical model vertical grid element size and the × indicates the location used for the model evaluation. Dashed line marks the mean canopy height.

Appendix S2. RAFLES evaluation.

The observed dispersal kernels of two species, red maple and silver maple, obtained by (Katul *et al.*, 2005) on May 13, 2001 are used to evaluate the performance of RAFLES. Only the manual releases of spray-marked seed were considered. For statistical comparison, the histogram of simulated dispersal distances is binned with the same bin width as the field experiment (5 meters) and normalized by the total sample size. Only the seeds released from the height of 30 m are used for model evaluation because only from that height did the observed dispersal distributions populate more than 5 bins, which is the minimum needed for a significant comparison with the simulation results. A linear regression is used to compare the observed and simulated binned probabilities, only including bins where the observed probability is greater than 0.

Figure A2.1 presents the comparison between the observed and simulated kernels, including the minimum and maximum probabilities for each of the histogram bins among the 10 virtual-location replications. Overall, the model compares well with the observations, meaning that the observations are within the bounds simulated by the model. For silver maple (terminal fall velocity, v_t = 1.1 m/s), we obtained a linear regression expressed by: Simulated = 1.23 × Observed - 0.04 (r^2 = 0.85; significance P = 0.003) with mean dispersal distance of 6.72 m for simulated data and 10.25 m for observed data. For red maple (v_t = 0.67 m/s), we obtained: Simulated = 0.74 × Observed + 0.04 (r^2 = 0.60; significance P = 0.040) with mean dispersal distance of 12.84 m for simulated data and 13.25 m for observed data. The regression slopes where not significantly different than 1. Compared to observed kernels, the simulated kernels have a

lower number of seeds at the far end of the tail and the means of the simulated kernels are skewed to the left, towards shorter dispersal. These differences could result from various factors. Although RAFLES accounts for 3D canopy heterogeneity, it only models the statistical properties of the canopy and does not explicitly simulate the location of the tower and adjacent trees where the field experiment took place. Also, as discussed above, the simulated atmospheric conditions are similar to those on the field experiment day but are not identical to those at the release time. The lower number of seeds at the very far end of the simulated tail can be explained by the lack of variability in terminal velocity in the model. It is also possible that an observational bias contributes to the differences between the modes of the observed and simulated dispersal kernels.

References

Katul, G.G., Porporato, A., Nathan, R., Siqueira, M., Soons, M.B., Poggi, D., Horn, H.S., & Levin, S.A. (2005) Mechanistic analytical models for long-distance seed dispersal by wind. *American Naturalist*, **166**, 368-381.

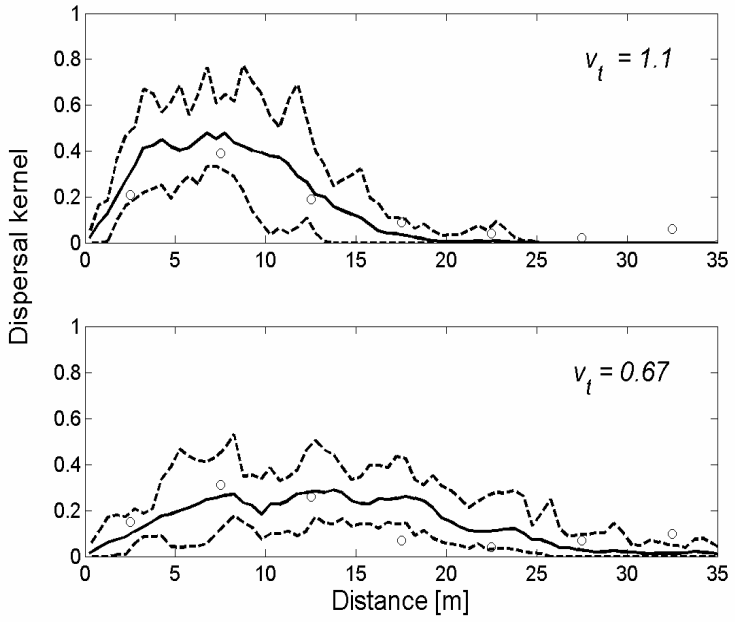

Figure A2.1. Dispersal kernels simulated (solid line) and observed by (Katul *et al.*, 2005) (open circles) for two wind dispersed species released from a height of 30 meters inside a

39-m high canopy. Dashed lines indicate the minimum and maximum obtained in the simulation.